


---

# COMPUTATIONAL ANALYSIS FOR COMPETITION FLOWS IN ARTERIOVENOUS FISTULAS BASED ON NON-CONTRAST MAGNETIC RESONANCE IMAGING

---

**Surabhi Rathore\***  
Mathematics Area, mathLab,  
SISSA, International School for Advanced Studies,  
via Bonomea 265,  
Trieste 34136, Italy

**Hironobu Sugiyama**  
Auckland City Hospital,  
Private Bag 92024,  
Auckland 1142, New Zealand

 **Hiroshi Suito†**  
Mathematical Science Group,  
Advanced Institute for Materials Research,  
Tohoku University, 2-1-1 Katahira,  
Aoba-ku, Sendai 980-8577, Japan

## ABSTRACT

**Introduction:** Characteristics of hemodynamics strongly affect the patency of arteriovenous fistula (AVF) in hemodialysis patients. Because of pressure balance changes among arteries after AVF construction, regurgitating flow occurs in some patients.

**Methods:** Based on phase-contrast MRI measurements, flow types around the anastomotic site are classified to the three different types of splitting, merging, and one-way, where merging type incorporates regurgitating flow. We have performed computational simulations to analyze characteristic differences among these types.

**Results:** In the merging type, a characteristic spiral flow is observed in AVF causing strong wall shear stress and large pressure drop, whereas the splitting type shows a smooth flow and gives a smaller pressure drop. The one-way case is intermediate between splitting and merging types.

**Conclusion:** Regurgitation brings about high wall shear stress near the anastomotic site because of instabilities induced by merging phenomena, for which type careful follow-up examinations are regarded as necessary.

**Keywords** Arteriovenous fistula · Hemodialysis · Phase-contrast MRI · Regurgitation · Wall shear stress

## 1 Introduction

End-stage renal disease (ESRD), a pathological condition in which kidney efficiency drops and low functionality persists, has been recognized worldwide as a severe chronic disease [1, 2]. National Kidney Foundation (NKF) Kidney Disease Outcomes Quality Initiative (K/DOQI) guidelines suggest hemodialysis as the preferred treatment for ESRD patients [3]. Vascular access (VA) is necessary to provide a long-patency hemodialysis. The most commonly used VA

---

\*This work was done at **Mathematical Science Group, Advanced Institute for Materials Research, Tohoku University, 2-1-1 Katahira, Aoba-ku, Sendai 980-8577, Japan**

†Corresponding Author. Email: [hiroshi.suito@tohoku.ac.jp](mailto:hiroshi.suito@tohoku.ac.jp)

is the arteriovenous fistula (AVF) proposed by Brescia et al. [4], which is created surgically between an artery and a vein. A sufficient rate of blood flow required for hemodialysis can be achieved by the pressure difference between these blood vessels. Nevertheless, reduction of the necessary blood flow rate sometimes occurs, which is responsible for AVF failure, as discussed in clinical reports [5, 6]. Even with recent clinical advances, not all the precise mechanisms and factors including maturation, constriction, and occlusion are known. Although these predictive factors are debatable, most VA stenoses are known to occur near the anastomotic site of AVF. They are caused by neointimal hyperplasia [7].

The mortality rate of dialysis patients is significantly higher than that of healthy individuals, as reported by the Japanese Society for Dialysis Therapy (JSDT) [8]. Several bodies of evidence have shown AVF to be superior to other VAs such as the arteriovenous graft (AVG) and catheters in terms of patency and complications, although clinical studies [9, 10] report that AVF might not necessarily be the most superior VA for elderly patients. Those with underlying diseases such as diabetes or hypertension are more likely to have blood vessel difficulties leading to primary failure of the AVF. Furthermore, primary failure in some cases might occur in AVF compared to AVG, as described in one earlier report [11]. To select appropriate treatments for different patient situations, algorithms for prediction that use scoring of the maturity of AVF and which use choosing between AVF or AVG have been proposed [12–15].

The morphology of the anastomotic sites of an AVF strongly affects the local hemodynamics within the AVF, where strong arterial blood flow dynamics exert dramatic effects on vein flow dynamics [16, 17]. In clinical evaluations for hemodynamics through AVFs, ultrasonography is a widely available, inexpensive, and noninvasive option, although the image quality depends heavily on the skills of operators [18–21]. In some cases, CT scans with contrast agents, which might adversely affect chronic renal failure, are used to acquire accurate morphological information related to AVFs. Other non-invasive options are magnetic resonance imaging (MRI), which is useful without a contrast agent and which provides accurate anatomical information, as reported from an earlier study [22].

Using such imaging techniques, several computational studies have been undertaken to elucidate the local hemodynamics within AVF [23–27]. These studies have provided a comprehensive understanding of hemodynamics within AVFs and have revealed direct correlation between altered wall shear stress (WSS) patterns and local vessel damage. Browne et al. [28] compared the in-vivo pressure distribution in AVF with numerical models. They reported a significant pressure drop across the fistula because of the flow instabilities at the anastomotic site. In some cases, fistula maturation depends on the anastomotic angle between an artery and a vein. This surgical factor relies on the expertise of surgeons. One earlier study [29] has demonstrated the importance of anastomotic angles on the blood flow dynamics. That study observed more disturbed flow for the larger anastomotic angle than for the smaller anastomotic angle. Bozzetto et al. [30] investigated the flow dynamics in different AVF geometries depending on the anastomotic site location. The assumption of wall deformation would greatly complicate the problem and would require the mechanical properties of the vessel wall. However, when compliant walls are considered, the flow fields are reportedly not greatly affected compared to the rigid wall [31]. As described in an earlier report [32], some patients experience blood flow regurgitation because of changes in pressure balance between the arteries, which affects the flow dynamics at the anastomotic sites. Surabhi et al. [33] described detailed three-dimensional flow field structures produced because of regurgitation from another artery.

This study explores the complex flow structures, WSS, and pressure distributions using medical imaging technologies such as MRI and phase-contrast MRI (PC-MRI) with regurgitating flow from the distal artery. The stabilized finite element method is used to solve the incompressible and unsteady Navier–Stokes equations which govern blood flow. Several complex blood flow characteristics have been computed. The structure of this paper comprises the following: Section 2 presents materials and methods, including the construction of AVF geometries using medical imaging data, computational procedures, and flow conditions. Section 3 presents the computational findings. Relevant discussion is presented in Section 4 with conclusions inferred from those results.

## 2 Materials and Methods

### 2.1 Patient-specific data

Institutional review board (IRB) approval was obtained from Akashi Medical Center Hospital (#2020 – 12) and the Tohoku University School of Medicine (#2020 – 1 – 511) in accordance with the Declaration of Helsinki for the conduct of this study. We evaluated three patients who had undergone AVF surgery in their wrist area. The underlying diseases were hypertension, diabetes, nephrosclerosis, and IgA nephropathy. End-to-side anastomosis has been performed in all candidates through surgery between the end of a vein and the side of an artery [34]. The evaluation was done one week after surgery. Relaxation Enhanced Angiography without Contrast and Triggering (REACT) method was used because it requires no conditions such as a high inflow rate, magnetic field homogeneity (fat suppression effect), or gated electrocardiogram. Other imaging techniques, such as Trigger Angiography Non-Contrast Enhance (TRANCE) and Time of flight angiography (TOF), which have prerequisites, are usually used for non-contrast shunt angiography, but they were not used for this study.

MRI medical imaging data of the targeted fistulas using the REACT method are provided in Digital Imaging and Communications in Medicine (DICOM) format. The extracted three-dimensional solid surfaces of AVF geometries are presented in Fig. 1. The configuration of these considered geometries consists of three parts connected at the anastomotic site presented in Fig. 1: the proximal artery (PA), distal artery (DA), and fistula vein (FV). Both PA and DA are parts of the radial artery. Therefore, three boundaries in our configuration other than the vessel wall boundary  $\Gamma_{wall}$  are included:  $\Gamma_{PA}$ ,  $\Gamma_{DA}$ , and  $\Gamma_{FV}$ .

We selected three patient-specific AVFs and designated these fistula geometries depending on their respective flow directions in DA as *Splitting* (S), *Merging* (M), and *One-way* (O) cases.

- **Case S:** The blood flow comes in from PA and splits into FV and DA.
- **Case M:** The blood flows coming in from PA and DA merge at the anastomotic site and pass out through FV. Incoming flow from DA is known as regurgitation, which occurs because of the change of pressure balance throughout the arterial system consisting of radial and ulnar arteries, and the palmar arch, by the construction of arteriovenous fistula.
- **Case O:** In this case, the DA flow is, quantitatively speaking, very small, indicating that the incoming flow from PA almost passes simply through FV. Aside from that, the small flow in DA causes some disturbances in the main flow from PA to FV.

### 2.2 Flow governing equations and computational procedures

We have considered blood as a Newtonian fluid, the flow of which is governed by unsteady, incompressible Navier–Stokes equations given below as

$$\begin{aligned}
 \rho (\mathbf{u}_{,t} + \mathbf{u} \cdot \nabla \mathbf{u}) - \nabla \cdot \boldsymbol{\sigma} &= \mathbf{0} && \text{in } \Omega \times (0, T), \\
 \nabla \cdot \mathbf{u} &= 0 && \text{in } \Omega \times (0, T), \\
 \mathbf{u} &= \mathbf{u}_g && \text{on } \Gamma_g \times (0, T), \\
 \boldsymbol{\sigma} \cdot \mathbf{n} &= \mathbf{0} && \text{on } \Gamma_h \times (0, T), \\
 \mathbf{u}(\mathbf{x}, 0) &= \mathbf{0} && \text{on } \Omega \times \{0\},
 \end{aligned} \tag{1}$$

where  $\Omega \subset \mathbf{R}^3$  is the spatial domain with the boundary  $\Gamma = \Gamma_g \cup \Gamma_h$ , which is defined as a disjoint union of essential and natural boundary conditions. Here,  $\mathbf{u}$  and  $\mathbf{n}$  respectively denote the velocity vector and the unit outward normal vector on the boundary  $\Gamma$ . Also,  $\boldsymbol{\sigma} = (-p\mathbf{I} + 2\mu\boldsymbol{\epsilon}(\mathbf{u}))$  is the stress tensor with the strain-rate tensor  $\boldsymbol{\epsilon}(\mathbf{u}) = \frac{1}{2}(\nabla \mathbf{u} + \nabla \mathbf{u}^T)$ , where  $p$ ,  $\mu$ , and  $\mathbf{I}$  respectively denote the pressure, viscosity, and identity tensor. At each boundary, flow velocity profile  $\mathbf{u}_g(t)$  is given. The vessel wall is regarded as rigid.

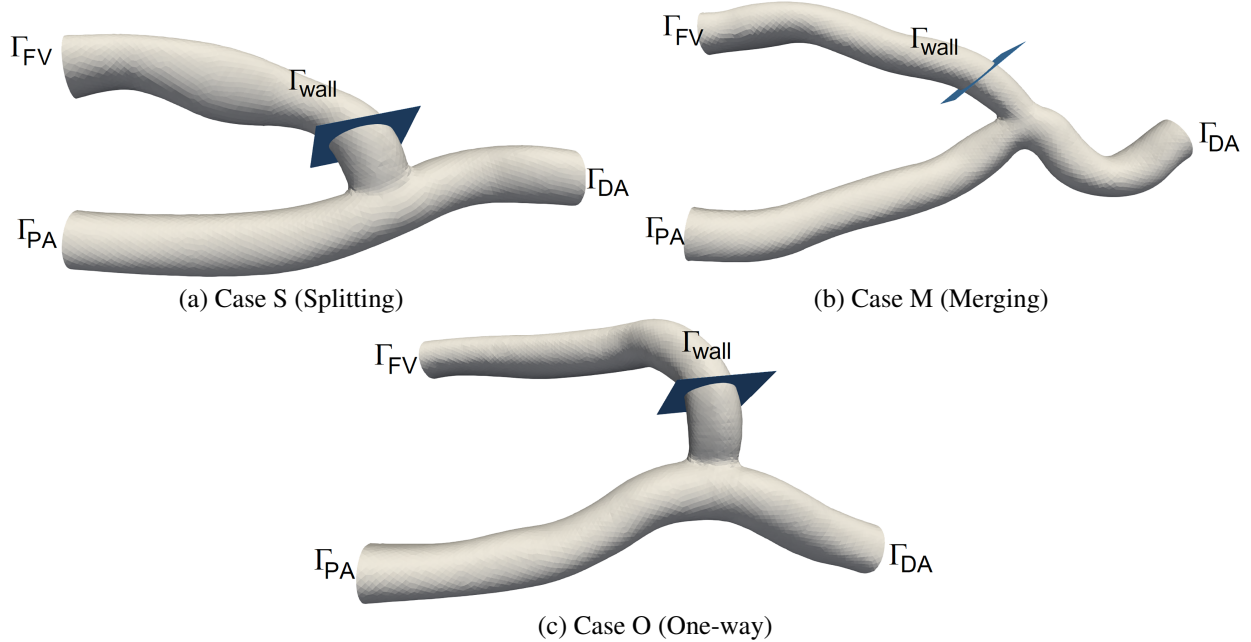


Figure 1: Extracted 3D arteriovenous fistula models with planes in fistula veins.

Equation 1 with complex geometries is solvable numerically using Galerkin finite element methods. However, such formulations are usually associated with potential numerical instabilities [35]. Tezduyar et al. [36, 37] proposed stabilized finite element formulations for incompressible fluid flows. We used the streamline upwind Petrov–Galerkin (SUPG) and pressure stabilizing Petrov–Galerkin (PSPG) methods [36, 37] for discretizing Eq. 1. Spatial domain  $\Omega$  is discretized into the elements  $\Omega_e = 1, 2, \dots, n_{el}$ , where  $n_{el}$  represents the number of elements. Details of computational procedures used for this study are the same as those described for an earlier study [33].

For computational simulations, blood density ( $\rho$ ) and blood viscosity ( $\mu$ ) are taken respectively as  $1060.0 \text{ kg/m}^3$  and  $2.66 \times 10^{-3} \text{ Ns/m}^2$ . Periodicities of the flow fields have been examined by computing the flow fields for several heart periods to avoid effects of initial conditions because we have no clear information about them. We decided to adopt the flow fields in the third period, where the effects of the initial conditions can be regarded as negligible. Geometries of three cases have been discretized into 38,499, 493,561, and 64,455 nodes and 206,407, 263,841, and 339,797 elements, respectively, for the S, M, and O cases. Time step length of  $\Delta t = 2 \times 10^{-4} \text{ s}$  was adopted. The sparse non-symmetric system of linear equations resulting from discretization of the governing equations is solved using the GPBi-CG method, as discussed in earlier reports [38, 39].

### 2.3 Flow conditions using PC-MRI

We have used PC-MRI measurement data to obtain boundary conditions for three inlet and outlet boundaries  $\Gamma_{PA}$ ,  $\Gamma_{DA}$ , and  $\Gamma_{FV}$ . The flow rates  $Q_{PA}(t)$  and  $Q_{DA}(t)$  are used respectively at boundaries  $\Gamma_{PA}$  and  $\Gamma_{DA}$ . We set  $\Gamma_{FV}$  as a traction-free boundary, which means that we do not need flow rate data at  $\Gamma_{FV}$ . We have adopted a rectification procedure for PC-MRI measurements in this study. Because, in measurements by PC-MRI, some flow rates include certain fluctuations, which are attributable to thrilling of vessels. Such non-physiological fluctuations cause severe instabilities in computational simulations. To overcome such difficulties, we use the mass conservation law within our target vessels portion, where the (sum of) incoming flow must be equal to the (sum of) outgoing flow.

$$Q_{PA} + Q_{DA} + Q_{FV} = 0.$$



In fact, for M and O cases, where flow rate data at  $Q_{DA}$  are fluctuating significantly, we neglect the MRI-measured flow rate profiles for DA and calculate it as

$$Q_{DA} = -Q_{FV} - Q_{PA},$$

where the negative sign of the flow rate represents incoming flow, whereas the positive sign represents outgoing flow. Rectified flow rates used as boundary conditions for computational simulations are presented in Fig. 2.

In case S, the PA flow is divided approximately equally into FV and the DA presented in Fig. 2(a). This flow type was discussed as Type 2 (anastomotic portion to distal) in an earlier report [32]. In case M, flows in PA and DA traveled together to the fistula vein, as presented in Fig. 2(b). The flow direction of DA is reversed (inward) to the anastomotic site, which might be attributable to ulnar arterial flow via the arterial arch in the palm. Such regurgitating phenomena have been discussed extensively as Type 1 (distal to anastomotic portion) [32]. In case O, the volume of radial artery was sufficient to maintain the volume of the vein presented in Fig. 2(c). Results show that the flow in the distal artery is very small and show that it changes the direction inlet or outlet.

### 3 Results

#### 3.1 Characteristics of flow fields in the AVFs

Figure 3 shows instantaneous streamlines at the maximum inflow at  $t = 2.097$  s,  $t = 1.955$  s, and  $t = 1.832$  s of the third heart period, respectively, for the S, M, and O cases, where the streamline colors represent velocity magnitudes.

In case S presented in Fig. 3(a), the blood flows coming in from PA and going out from both FV and DA generate a recirculation zone at the inner side of the vein near the anastomotic site, whereas another disturbance is seen in FV because of the radius change of the vein. In case M presented in Fig. 3(b), the blood flows coming in from both PA and DA merge at the anastomotic site and go through FV. Strong flow is apparent along the FV wall in a spiral shape caused by the merging from PA and DA. In case O presented in Fig. 3(c), the blood flow is coming in mainly from PA. The small regurgitation from DA plays a role in disturbing the main flow of FV because circulation around the vessel axis is apparent in FV near the anastomotic site. We have also observed lower velocity magnitude circulation regions in DA because of marked changes in the DA flow direction.

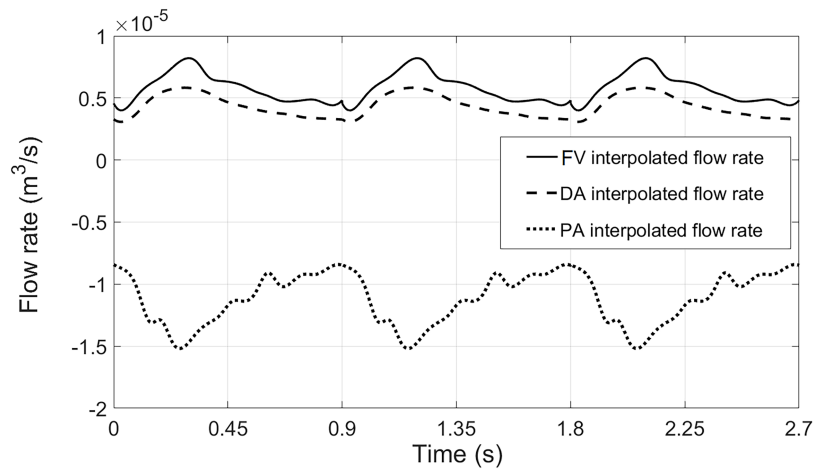
#### 3.2 Wall shear stress and pressure distributions

WSS exerted on the endothelial surface of blood vessels is defined as

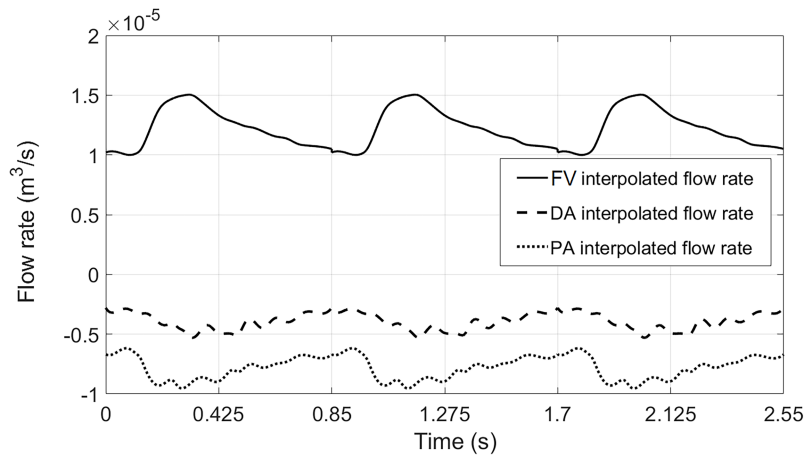
$$\tau_w = \mathbf{t} - (\mathbf{t} \cdot \mathbf{n}) \mathbf{n}, \quad (2)$$

where  $\mathbf{t}$  is a traction vector computed from the stress tensor and surface normal vector, as  $\mathbf{t} = \sigma \mathbf{n}$ . Figure 4 presents the WSS distributions at the time steps of the maximum inflow rates for cases S, M, and O. In case M portrayed in Fig. 4(b), strong WSS is apparent throughout FV which results from the strong flow merged from PA and DA. In case O portrayed in Fig. 4(c), strong WSS is confined near the anastomotic site which apparently results from strong circulation generated by the disturbance from DA, as depicted in Fig. 3(c). In case S portrayed in Fig. 4(a), WSS is maintained at a lower level, even in neighboring areas around the anastomotic site.

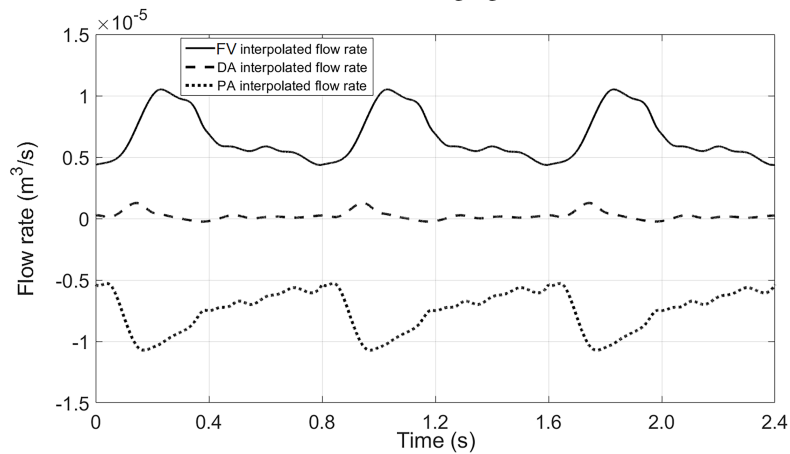
Figure 5 presents the magnitude of velocities on the cross-sectional planes indicated in Fig. 1 in FVs near the anastomotic sites, respectively, for cases S, M, and O. In case M in Fig. 5(b), a strong flow exists because of merging from PA and DA, which generates a large velocity gradient near the vessel wall and exerts strong WSS on the vessel wall. Additionally, in case O presented in Fig. 5(c), the larger velocity gradient is shown near the vessel wall compared with case S in Fig. 5(a). A critical difference between cases S and M is that the strong flow is confined in the half (lower part of Fig. 5(b)) of cross-section in case M, whereas the flow is distributed more uniformly over the cross-section in case S. Case O is intermediate between cases M and S.



(a) Case S (Splitting)



(b) Case M (Merging)



(c) Case O (One-way)

Figure 2: Flow rates for the proximal artery (PA), distal artery (DA), and fistula vein (FV) for the Splitting (S), Merging (M), and One-way (O) cases. A positive sign denotes outgoing flows; negative signifies incoming.

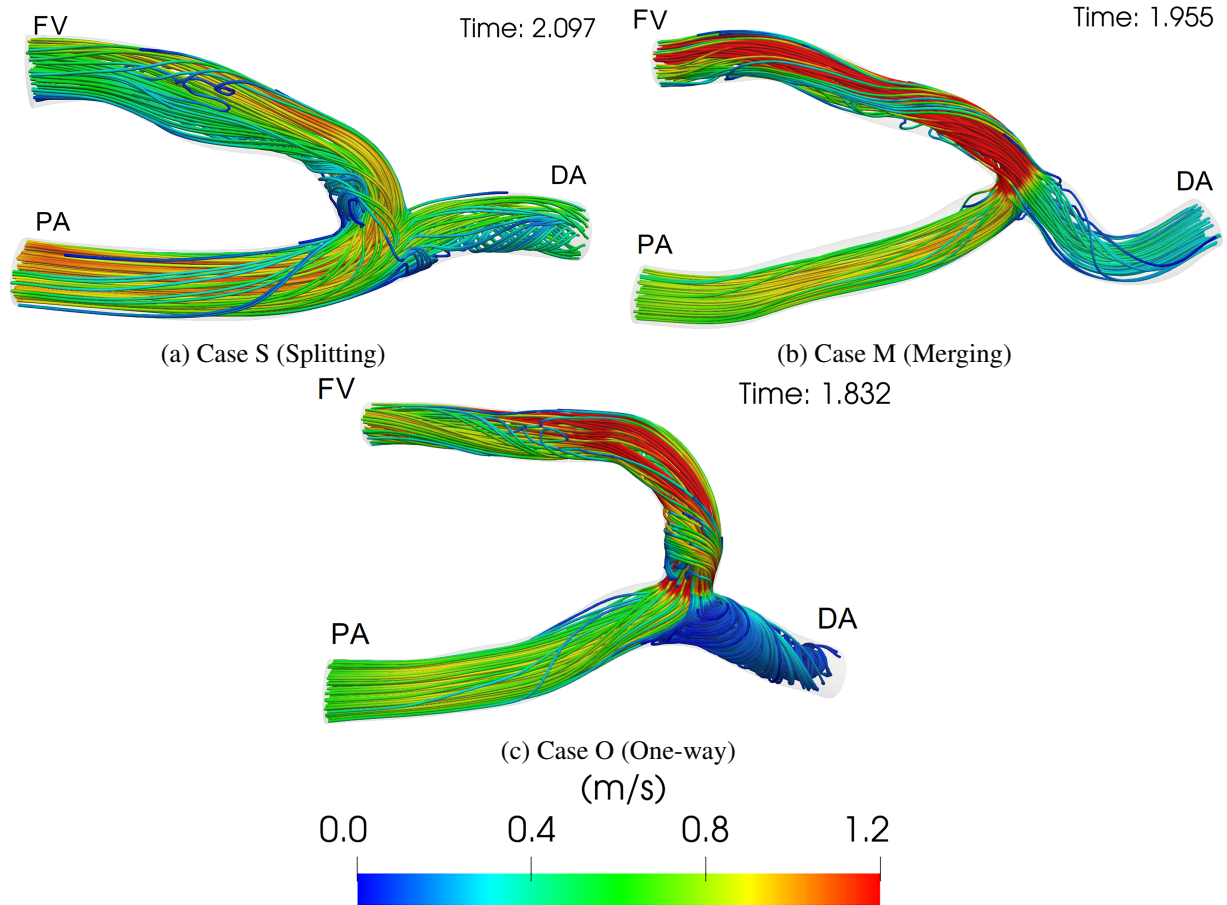


Figure 3: Instantaneous streamlines for the S, M, and O cases.

Figure 6 presents pressure difference distributions, where the reference pressure value is set at zero on the outflow boundary; the pressure difference is higher in cases M and O than in case S. In case O depicted in Fig. 6(c), a higher-pressure region arises near the anastomotic site in FV, which is attributable to the circulation induced by a small disturbance through regurgitation from DA.

### 3.3 Energy loss and pressure drops

Figure 7 presents the spatially averaged pressure history for one heart period in cases S, M, and O, respectively, which shows that the pressures change greatly in cases M and O compared with case S. Differences of time-averaged pressures between inflow and outflow boundaries are 45 mmHg, 130 mmHg, and 90 mmHg, respectively, in cases S, M, and O. The pressure drops between inflow and outflow boundaries are related strongly to the total flow rate as well as disturbances in the flow fields near the anastomotic site. The disturbed flow in FV near the anastomotic site in case O seems to contribute to larger pressure drop in this case. From the perspective of energy balance, a larger pressure drop signifies a stronger energy loss, which affects degeneration of endothelial cells of vessel walls through the effects of WSS [17, 27, 40].

## 4 Discussion

Patients with ESRD often need hemodialysis with appropriate VAs, of which the most preferred type is AVFs. Prolonged patency of the AVFs is strongly anticipated but approximately 50% of AVFs fail sometimes after surgery, causing adverse clinical outcomes [41, 42]. The underlying failure mechanism remains to be elucidated, but the most

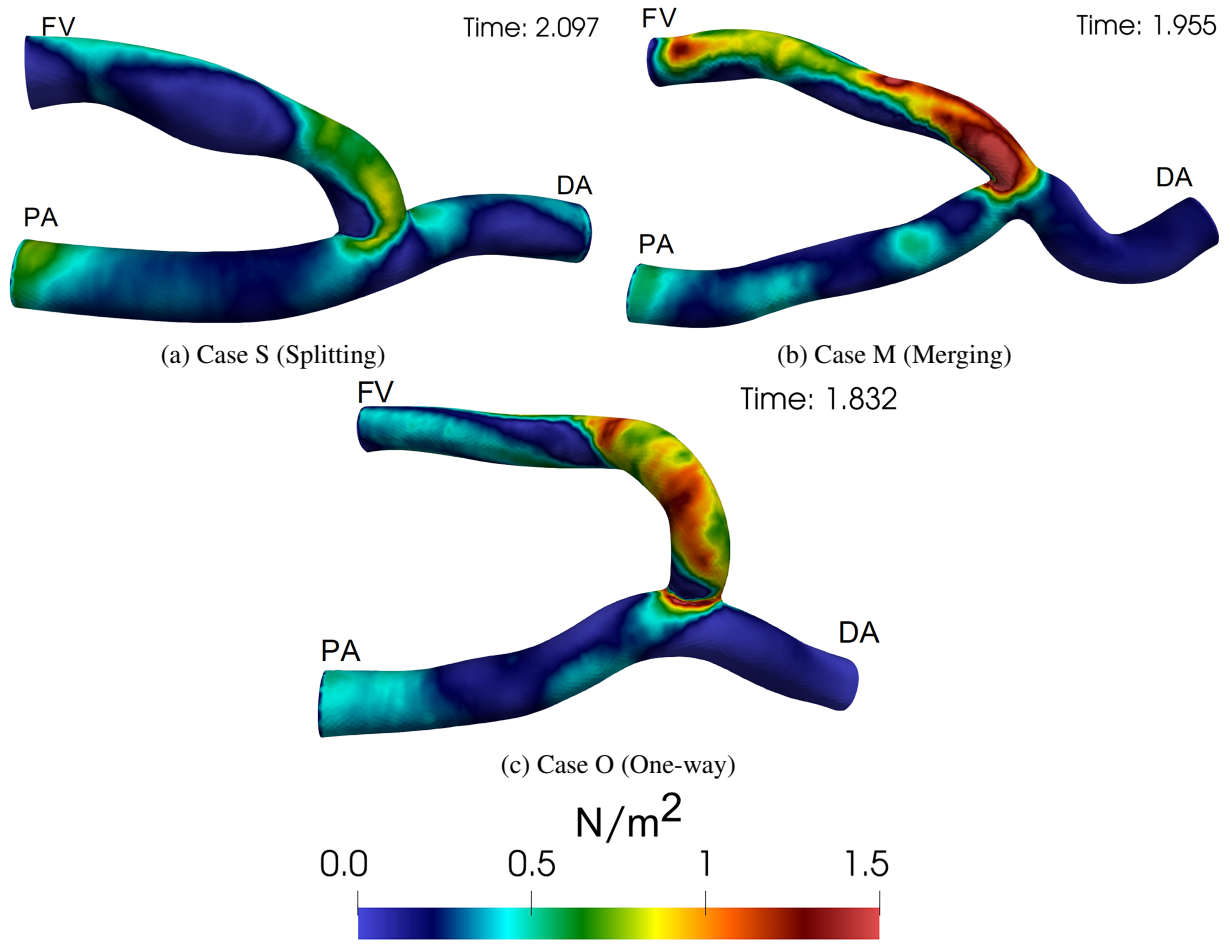


Figure 4: Wall shear stresses for the S, M, and O cases.

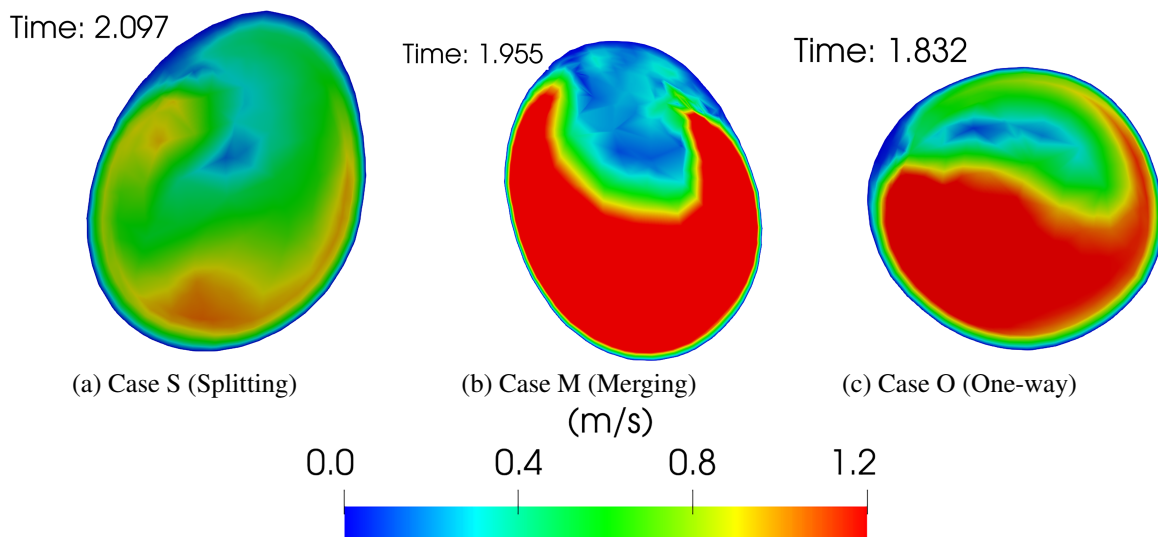


Figure 5: Velocity magnitudes on cross sections for the S, M, and O cases.

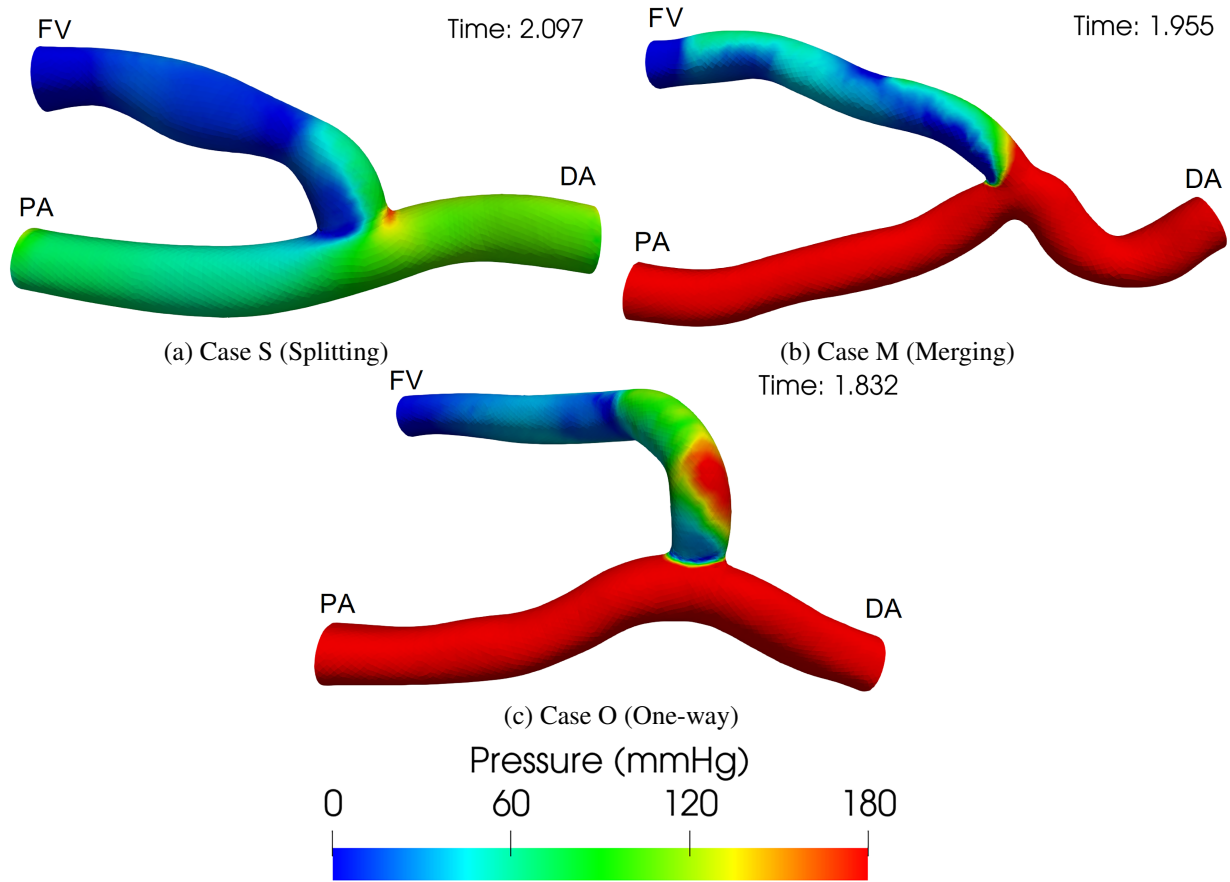


Figure 6: Pressure differences for the S, M, and O cases.

common reason for failure is the formation of intimal hyperplasia, which reduces the size of the lumen and flow rate within AVF. For this study, we have considered three patient cases including the regurgitating flow case, in which the blood flow regurgitates to the radial artery from the ulnar artery through the palmar arch because of the changes in pressure balance between radial and ulnar arteries. Although we were unable to measure the actual flow rate in the distal part (DA) correctly because of thrill of the vessels, we have applied the mass conservation law to obtain more accurate flow rate data.

In case M (merging), the regurgitating flow strongly influences the main flow at the anastomotic site. The strong flow adheres progressively to the outer wall of FV, elevating the shear stress there as presented in Fig. 5(b). In case O (one-way), a small flow from DA disturbs the main flow in FV. Circulations around the vessel axis are apparent in FV near the anastomotic site shown in Fig. 3(c). These results exhibited that the M case with strong regurgitation is subjected to quite high shear stresses, which concurs with results reported from several earlier studies [23–27], and indicating that vessel walls are more vulnerable to vascular damage when the WSS is high or oscillating. Disturbances of flow at venous anastomosis of AVFs are also associated with vascular remodeling described in these reports [6, 40]. It has been observed that circulation in the venous side at anastomotic site, caused by regurgitating flow, is also responsible for significant pressure drops between the inflow and outflow boundaries for M and O cases. We have observed that venous segments of these AVFs showed much lower blood pressure levels than the arterial segments depicted in Fig. 6. These computational results are in line with those of earlier studies [28–30].

AVF patients undergoing hemodialysis usually have complicated hemodynamic conditions. The surgical construction of the anastomosis between an artery and a vein affects the flow dynamics there because of local morpho-

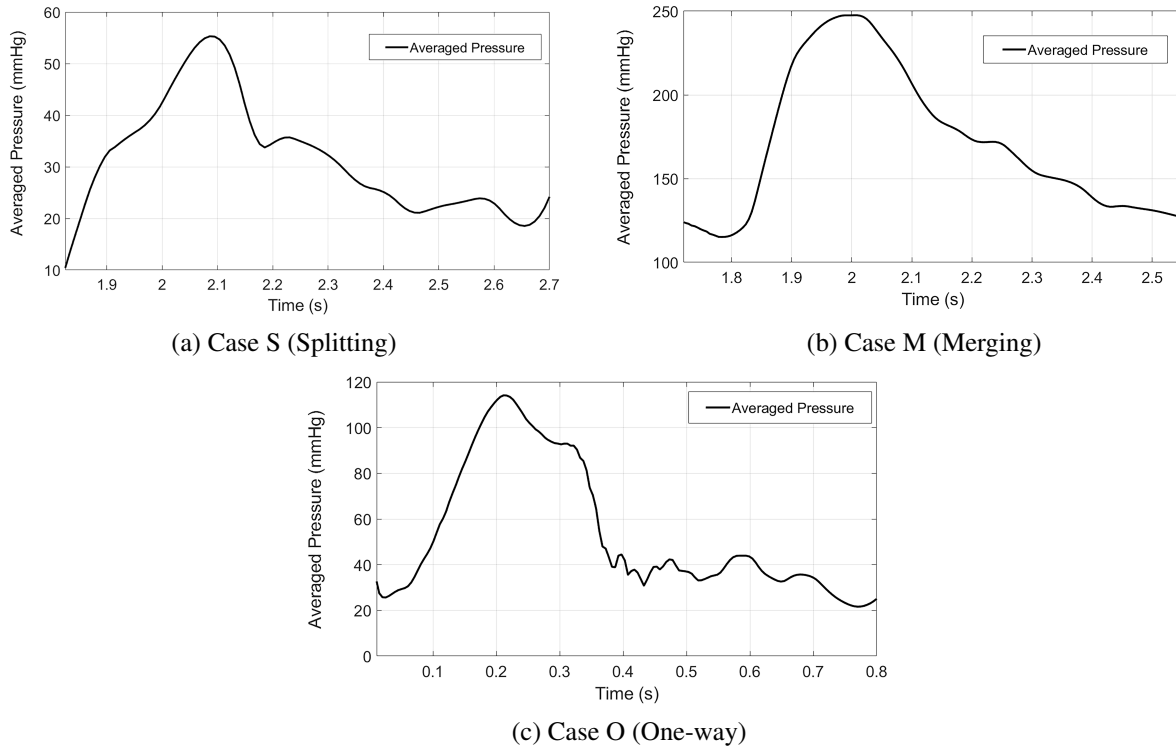


Figure 7: Spatially Averaged Pressures for the S, M, and O cases.

gies of the blood vessels and because of global pressure distribution changes. This paper has presented computational analysis using patient-specific morphologies and flow conditions immediately after construction of AVFs from fluid dynamics points of view. As time goes on after surgery, deformation and pressure balance in the vessels network might change, which finally brings about occlusion of vessels. The present study has the following limitations. We considered a small number of patient cases that represent flow conditions of specific types. A broad scope of AVF morphologies and regurgitating patterns must be considered in future works. Moreover, the morphologies adopted for this study were taken only a week after the surgery. Morphologies and flow conditions might change after a long time, which is beyond the scope of the present study.

The results presented herein suggest important differences between different morphologies and flow conditions including regurgitations. Regurgitation brings about high wall shear stress near the anastomotic site because of instabilities induced by merging phenomena, for which type careful follow-up examinations are regarded as necessary. These findings might therefore provide insights into reasons for occlusions and maturation failures, along with indications for surgery planning.

### Conflict of interest

We hereby declare that the authors have no potential conflict of interest related to this study.

### Ethical Statement

Institutional review board (IRB) approval was obtained from Akashi Medical Center Hospital and the Tohoku University School of Medicine in accordance with the Declaration of Helsinki.



## Funding

This work was supported by JST CREST with Grant Number: JPMJCR15D1, Japan.

## References

- [1] Elliott M Levy, Catherine M Viscoli, and Ralph I Horwitz. The effect of acute renal failure on mortality: a cohort analysis. *Jama*, 275(19):1489–1494, 1996. doi:10.1001/jama.1996.03530430033035.
- [2] CY Hsu, JD Ordonez, GM Chertow, D Fan, CE McCulloch, and AS Go. The risk of acute renal failure in patients with chronic kidney disease. *Kidney international*, 74(1):101–107, 2008. doi:10.1038/ki.2008.107.
- [3] Charmaine E Lok, Thomas S Huber, Timmy Lee, Surendra Shenoy, Alexander S Yevzlin, Kenneth Abreo, Michael Allon, Arif Asif, Brad C Astor, Marc H Glickman, et al. Kdoqi clinical practice guideline for vascular access: 2019 update. *American Journal of Kidney Diseases*, 75(4):S1–S164, 2020. doi:10.1053/j.ajkd.2019.12.001.
- [4] Michael J Brescia, James E Cimino, Kenneth Appel, and Baruch J Hurwich. Chronic hemodialysis using venipuncture and a surgically created arteriovenous fistula. *New England Journal of Medicine*, 275(20):1089–1092, 1966. doi:10.1056/NEJM196611172752002.
- [5] Ilse Van Tricht, Dirk De Wachter, Jan Tordoir, and Pascal Verdonck. Hemodynamics and complications encountered with arteriovenous fistulas and grafts as vascular access for hemodialysis: a review. *Annals of biomedical engineering*, 33:1142–1157, 2005. doi:10.1007/s10439-005-5367-X.
- [6] Mark F Fillinger, Emanuel R Reinitz, Robert A Schwartz, Dennis E Resetarits, Andrew M Paskanik, and Carl E Bredenberg. Beneficial effects of banding on venous intimal-medial hyperplasia in arteriovenous loop grafts. *The American journal of surgery*, 158(2):87–94, 1989. doi:10.1016/0002-9610(89)90353-X.
- [7] William E Stehbens and Alistair M Karmody. Venous atherosclerosis associated with arteriovenous fistulas for hemodialysis. *Archives of Surgery*, 110(2):176–180, 1975. doi:10.1001/archsurg.1975.01360080042006.
- [8] Akira Mima. Hemodialysis vascular access dysfunction: molecular mechanisms and treatment. *Therapeutic Apheresis and Dialysis*, 16(4):321–327, 2012. doi:10.1111/j.1744-9987.2012.01066.x.
- [9] Michael Allon. Vascular access for hemodialysis patients: new data should guide decision making. *Clinical journal of the American Society of Nephrology: CJASN*, 14(6):954, 2019. doi:10.2215/CJN.00490119.
- [10] Andrea K Viecelli and Charmaine E Lok. Hemodialysis vascular access in the elderly—getting it right. *Kidney international*, 95(1):38–49, 2019. doi:10.1016/j.kint.2018.09.016.
- [11] Ivan D Maya, Jeremy C O’Neal, Carlton J Young, Jill Barker-Finkel, and Michael Allon. Outcomes of brachiocephalic fistulas, transposed brachiobasilic fistulas, and upper arm grafts. *Clinical journal of the American Society of Nephrology: CJASN*, 4(1):86, 2009. doi:10.2215/CJN.02910608.
- [12] Robert S Brown, Bhanu K Patibandla, and Alexander S Goldfarb-Rumyantsev. The survival benefit of “fistula first, catheter last” in hemodialysis is primarily due to patient factors. *Journal of the American Society of Nephrology: JASN*, 28(2):645, 2017. doi:10.1681/ASN.2016010019.
- [13] Eduard HJ Voormolen, Abdelkarime Khodadade Jahrome, Lambertus W Bartels, Frans L Moll, Willem P Mali, and Peter J Blankestijn. Nonmaturation of arm arteriovenous fistulas for hemodialysis access: a systematic review of risk factors and results of early treatment. *Journal of vascular surgery*, 49(5):1325–1336, 2009. doi:10.1016/j.jvs.2008.11.059.
- [14] Charmaine E Lok, Michael Allon, Louise Moist, Matthew J Oliver, Hemal Shah, and Deborah Zimmerman. Risk equation determining unsuccessful cannulation events and failure to maturation in arteriovenous fistulas (reduce ftm i). *Journal of the American Society of Nephrology*, 17(11):3204–3212, 2006. doi:10.1681/ASN.2006030190.
- [15] Michael Allon and Charmaine E Lok. Dialysis fistula or graft: the role for randomized clinical trials. *Clinical journal of the American Society of Nephrology*, 5(12):2348–2354, 2010. doi:10.2215/CJN.06050710.
- [16] Domenico Santoro, Filippo Benedetto, Placido Mondello, Narayana Pipitò, David Barillà, Francesco Spinelli, Carlo Alberto Ricciardi, Valeria Cernaro, and Michele Buemi. Vascular access for hemodialysis: current perspectives. *International journal of nephrology and renovascular disease*, pages 281–294, 2014. doi:10.2147/IJNRD.S46643.
- [17] Leonard D Browne, Khalid Bashar, Philip Griffin, Eamon G Kavanagh, Stewart R Walsh, and Michael T Walsh. The role of shear stress in arteriovenous fistula maturation and failure: a systematic review. *PloS one*, 10(12):e0145795, 2015. doi:10.1371/journal.pone.0145795.

- [18] William H Bay, Mitchell L Henry, J Michael Lazarus, Nancy L Lew, Jie Ling, and Edmund G Lowrie. Predicting hemodialysis access failure with color flow doppler ultrasound. *American Journal of Nephrology*, 18(4):296–304, 1998. doi:10.1159/000013354.
- [19] Patrick Wiese and Barbara Nonnast-Daniel. Colour doppler ultrasound in dialysis access. *Nephrology Dialysis Transplantation*, 19(8):1956–1963, 2004. doi:10.1093/ndt/gfh244.
- [20] Christoph Schwarz, Christa Mitterbauer, Maryla Boczula, Thomas Maca, Martin Funovics, Georg Heinze, Matthias Lorenz, Josef Kovarik, and Rainer Oberbauer. Flow monitoring: performance characteristics of ultrasound dilution versus color doppler ultrasound compared with fistulography. *American journal of kidney diseases*, 42(3):539–545, 2003. doi:10.1016/S0272-6386(03)00786-8.
- [21] Bianca Visciano, Eleonora Riccio, Vincenzo De Falco, Antonino Musumeci, Ivana Capuano, Andrea Memoli, Antonella Di Nuzzi, and Antonio Pisani. Complications of native arteriovenous fistula: The role of color doppler ultrasonography. *Therapeutic Apheresis and Dialysis*, 18(2):155–161, 2014. doi:10.1111/1744-9987.12073.
- [22] Eoin A Murphy, Rose A Ross, Robert G Jones, Stephen J Gandy, Nicolas Aristokleous, Marco Salsano, Jonathan R Weir-McCall, Shona Matthew, and John Graeme Houston. Imaging in vascular access. *Cardiovascular engineering and technology*, 8:255–272, 2017. doi:10.1007/s13239-017-0317-y.
- [23] Bogdan Ene-Iordache, Lidia Mosconi, Giuseppe Remuzzi, and Andrea Remuzzi. Computational fluid dynamics of a vascular access case for hemodialysis. *J. Biomech. Eng.*, 123(3):284–292, 2001. doi:10.1115/1.1372702.
- [24] Z Kharboutly, M Fenech, JM Treutenaere, I Claude, and C Legallais. Investigations into the relationship between hemodynamics and vascular alterations in an established arteriovenous fistula. *Medical engineering & physics*, 29(9):999–1007, 2007. doi:10.1016/j.medengphy.2006.10.018.
- [25] Zaher Kharboutly, Valerie Deplano, Eric Bertrand, and Cecile Legallais. Numerical and experimental study of blood flow through a patient-specific arteriovenous fistula used for hemodialysis. *Medical engineering & physics*, 32(2):111–118, 2010. doi:10.1016/j.medengphy.2009.10.013.
- [26] Henricus JTAM Huijbrechts, Michiel L Bots, Frans L Moll, Peter J Blankestijn, et al. Hospital specific aspects predominantly determine primary failure of hemodialysis arteriovenous fistulas. *Journal of vascular surgery*, 45(5):962–967, 2007. doi:10.1016/j.jvs.2007.01.014.
- [27] Bogdan Ene-Iordache and Andrea Remuzzi. Disturbed flow in radial-cephalic arteriovenous fistulae for haemodialysis: low and oscillating shear stress locates the sites of stenosis. *Nephrology Dialysis Transplantation*, 27(1):358–368, 2012. doi:10.1093/ndt/gfr342.
- [28] Leonard D Browne, Philip Griffin, Khalid Bashar, Stewart R Walsh, Eamon G Kavanagh, and Michael T Walsh. In vivo validation of the in silico predicted pressure drop across an arteriovenous fistula. *Annals of biomedical engineering*, 43:1275–1286, 2015. doi:10.1007/s10439-015-1295-6.
- [29] Simone Stella, Christian Vergara, Luca Giovannacci, Alfio Quarteroni, and Giorgio Prouse. Assessing the disturbed flow and the transition to turbulence in the arteriovenous fistula. *Journal of biomechanical engineering*, 141(10):101010, 2019. doi:10.1115/1.4043448.
- [30] Michela Bozzetto, Bogdan Ene-Iordache, and Andrea Remuzzi. Transitional flow in the venous side of patient-specific arteriovenous fistulae for hemodialysis. *Annals of biomedical engineering*, 44:2388–2401, 2016. doi:10.1007/s10439-015-1525-y.
- [31] Iolanda Decorato, Zaher Kharboutly, Tommaso Vassallo, Justin Penrose, Cécile Legallais, and Anne-Virginie Salsac. Numerical simulation of the fluid structure interactions in a compliant patient-specific arteriovenous fistula. *International journal for numerical methods in biomedical engineering*, 30(2):143–159, 2014. doi:10.1002/cnm.2595.
- [32] Minoru Kikuchi, Ryo Ohtani, and Hiroshi Saito. Investigation of blood flow measurements using vascular access ultrasonography in the anastomotic distal portion of an arteriovenous fistula. *Japanese Journal of Medical Ultrasound Technology*, 43(1):34–42, 2018. doi:10.11272/jss.43.34.
- [33] Surabhi Rathore, Tomoki Uda, Viet QH Huynh, Hiroshi Suito, Toshitaka Watanabe, Hironobu Sugiyama, and D Srikanth. Numerical computation of blood flow for a patient-specific hemodialysis shunt model. *Japan Journal of Industrial and Applied Mathematics*, 38(3):903–919, 2021. doi:/10.1007/s13160-021-00469-9.
- [34] Klaus Konner. The anastomosis of the arteriovenous fistula—common errors and their avoidance. *Nephrology Dialysis Transplantation*, 17(3):376–379, 2002. doi:10.1093/ndt/17.3.376.
- [35] Jean Donea and Antonio Huerta. *Finite element methods for flow problems*. John Wiley & Sons, 2003.

- [36] Tayfun E Tezduyar. Stabilized finite element formulations for incompressible flow computations. *Advances in applied mechanics*, 28:1–44, 1991. doi:10.1016/S0065-2156(08)70153-4.
- [37] Tayfun E Tezduyar, Sanjay Mittal, SE Ray, and R Shih. Incompressible flow computations with stabilized bilinear and linear equal-order-interpolation velocity-pressure elements. *Computer Methods in Applied Mechanics and Engineering*, 95(2):221–242, 1992. doi:10.1016/0045-7825(92)90141-6.
- [38] Shao-Liang Zhang. Gpbi-cg: Generalized product-type methods based on bi-cg for solving nonsymmetric linear systems. *SIAM Journal on Scientific Computing*, 18(2):537–551, 1997. doi:10.1137/S1064827592236313.
- [39] Quang Huy Viet Huynh and Hiroshi Suito. A multi-gpu implementation of a parallel solver for incompressible navier-stokes equations discretized by stabilized finite element formulations (numerical analysis: New developments for elucidating interdisciplinary problems ii). *RIMS Kokyuroku*, 2037:149–152, 2017. doi:http://hdl.handle.net/2433/236868.
- [40] David N Ku, Don P Giddens, Christopher K Zarins, and Seymour Glagov. Pulsatile flow and atherosclerosis in the human carotid bifurcation. positive correlation between plaque location and low oscillating shear stress. *Arteriosclerosis: An Official Journal of the American Heart Association, Inc.*, 5(3):293–302, 1985. doi:10.1115/1.2895545.
- [41] Morton H Friedman, Owen J Deters, C Brent Barger, Grover M Hutchins, and Frank F Mark. Shear-dependent thickening of the human arterial intima. *Atherosclerosis*, 60(2):161–171, 1986. doi:10.1016/0021-9150(86)90008-0.
- [42] Jean-Marc Corpataux, Erik Haesler, Paolo Silacci, Hans Beat Ris, and Daniel Hayoz. Low-pressure environment and remodelling of the forearm vein in brescia–cimino haemodialysis access. *Nephrology Dialysis Transplantation*, 17(6):1057–1062, 2002. doi:10.1093/ndt/17.6.1057.